UNIVERSITÀ POLITECNICA DELLE MARCHE

FACOLTÀ DI INGEGNERIA

Corso di Laurea Magistrale in Ingegneria elettronica

ANALISI TEORICA E SPERIMENTALE DI PHASE-SHIFTERS BASATI SU METAMATERIALI PER APPLICAZIONI AD ALTA FREQUENZA

THEORETICAL AND EXPERIMENTAL ANALYSIS OF METAMATERIAL-BASED PHASE-SHIFTERS FOR HIGH-FREQUENCY APPLICATIONS

Relatore:
Prof. Luca Pierantoni

Tesi di Laurea di:
Athos Sonara

Correlatore:
Dr. Davide Mencarelli

Correlatore:
Dr. Mehmet Kaynak

ANNO ACCADEMICO 2021/2022

Contents

Abstract

Questa tesi ha lo scopo di sviluppare un modello teorico-computazione e le specifiche di progetto di phase-shifters basati su linee di trasmissione con metamateriali che operino nella banda 110-170 GHz. Lo studio di questi dispositivi si pone nell'ambito di una collaborazione tra il Dipartimento di Ingegneria dell'Informazione (DII) dell'UNIVPM e il centro di ricerca e produzione IHP Microelectronics GmbH. Grazie a questa collaborazione è stato possibile effettuare un confronto teorico-sperimentale tra risultati delle simulazioni e dati sperimentali ottenuti da misurazioni sul dispositivo realizzato. Esiste una vasta letteratura the tratta di phase-shifters con materiali tradizionali e relative applicazioni; il vantaggio nell'uso dei metamateriali consiste, in particolare, nella miniaturizzazione, nella riduzione del cross-talk e dell'accoppiamento capacitivo, e permette di realizzare dispositivi a basso consumo energetico. Dispositivi di questo tipo trovano molteplici applicazioni in sistemi dalla radiofrequenza (RF) alle onde millimetriche; infatti il phase-shifter è un componente fondamentale per la realizzazione di sistemi quali phased-array di antenne, dispositivi di accoppiamento, filtri tunabili, circolatori e altro. Il modello teorico si basa su una linea di trasmissione a microstriscia sopra un substrato di ossido di silicio, in cui vengono inserite coppie di celle risonanti ad accoppiamento elettrico (ELC). In base alle dimensioni e al numero delle celle inserite, l'onda elettromagnetica in propagazione nella microstriscia avrà un'interazione con le celle sottostanti che, a loro volta produrranno un campo che si accoppierà all'onda iniziale. La presenza delle celle nel dielettrico risulta in un materiale con indice di permittività negativo. È stato possibile ottenere dati da misurazioni sulle effettive linee di trasmissione prodotte, viene infatti descritto il processo di produzione in silicio-germanio (S_iG_e). Per rendere possibile la misurazione, la struttura è stata progettata con un'interfaccia coplanare con una successiva transizione a microstriscia, rendendo necessaria una calibrazione MRTL (Multi Thru-Reflect Line) della probe-station. Prima di passare alla modellazione, viene quindi esposta la procedura di misurazione e calibrazione dello strumento. La simulazione full-wave 3D è stata effettuata utilizzando COMSOL Multiphysics® e MATLAB®, tenendo conto delle dimensioni reali (spessore del substrato, dimensioni della linea) e delle specifiche dello stack tecnologico (caratteristiche dei materiali) IHP. Lo scopo è quello di ottenere curve teoriche dei parametri di Scattering da porre a confronto con quelle ottenute dalle misurazioni on-wafer. Si passa quindi al confronto teorico-sperimentale tra i dati ottenuti dalle misurazioni e quelli prodotti dal simulatore. Dal confronto emerge chiaramente che il modello teorico-numerico permette di predire le misure sperimentali con grande accuratezza. Vengono infine riportate le curve degli andamenti della fase, dai risultati è possibile osservare i valori di sfasamento al variare della dimensione e del numero delle celle presenti nel dielettrico. Il dispositivo realizzato è alla base dello sviluppo di un phase-shifter tunabile, di fondamentale importanza per la fabbricazione di array di antenne e altri dispositivi.

Introduction

Metamaterials have become an hot topic in recent years due to the vast application possibilities, focusing on achieving physical properties that do not exist in nature. The study of metamaterials opens up various researching fields especially in RF applications [1]. Examples of metamaterials include electromagnetic band gaps, artificial magnetic conductors, and double-negative or left handed materials. Such MMs with negative refractive index have found applications in wide range of microwave electronics and devices[2, 3]. Phase shifters are the key components in RF/MM-wave applications such as phased array radar systems and antennae[4], but also tunable filters, circulators and more. There's vaste literature of conventional phase shifters, realised using traditional materials [5, 6]; however, the advantages of using metamaterial devices are the miniaturization, the reduction of capacitive coupling and cross-talk, and the low power consumption, granting better performances in advanced microwaves systems. Recently, composite right/left-handed transmission lines have been used to design scaled devices. This thesis presents models of a phase-shifters, obtained adding couples of electrically-coupled LC resonator cells (ELC) embedded in S_iO_2 under a microstrip line to obtain an epsilon-negative metamaterial. These structures are produced in S_iG_e technology in IHP Microelectronics GmbH, a research center in close collaboration with the DII (Dipartimento di Ingegneria dell'Informazione). During an internship in said research center, it was possible to take on-wafer measurement of the fabricated devices to compare the experimental Scattering parameters with the theoretical results of the simulations. These full-wave 3D simulations were obtained in MATLAB® and COMSOL Multiphysics®, defining the dimensions and the material parameters considering the S_iG_e production process performed in IHP. After explaining the basic theory of metamaterials in chapter 1, the thesis presents the production process, the measurement protocol and the calibration method in chapter 2, the models used to simulate the device in chapter 3 and lastly, the theoretical-experimental comparison between the real measurement data and the simulation results in chapter 4.

Chapter 1

Metamaterials

1.1 General classification

A metamaterial is an artificial material designed to have physical properties that do not exist in nature. These properties are obtained by arranging specific microstructures called "atoms" or cells. Considering the electromagnetic properties (ε and μ), metamaterials can be divided in four different groups:

1. Double positive (DPS), materials that have $\varepsilon > 0$ and $\mu > 0$. This group represents the major part of the existing natural material.
2. Epsilon negative (ENG), materials that have $\varepsilon < 0$ and $\mu > 0$. This group is represented by plasmas.
3. Double negative (DNG), materials that have $\varepsilon < 0$ and $\mu < 0$. This group does not exist in nature and it is completely artificial.
4. Mu negative (MNG), materials that have $\varepsilon > 0$ and $\mu < 0$. This group is represented by ferrites.

Figure 1.1 shows the material classification. The refractive index of a material $n = \sqrt{\varepsilon_r \mu_r}$, depending on the type of material, could be both real or imaginary and positive or negative. In DPS and DNG materials the refraction index is real and all the waves can propagate, in ENG and MNG evanescent waves can be found because of the imaginary refraction index.

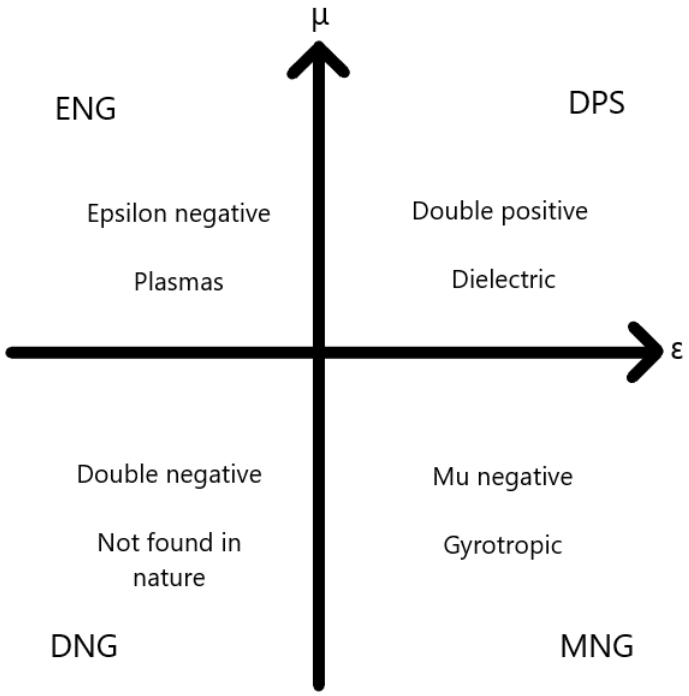

Figure 1.1: Metamaterial classification considering electromagnetic properties

1.2 ENG metamaterials

The dielectric permittivity of a plasma varies in frequency as shown in equation 1.1.

$$\varepsilon_r = 1 - \frac{(\omega_p^2)}{\omega^2} \tag{1.1}$$

The permittivity is positive for waves propagating above the plasma frequency (ω_p) and negative below. A simple design for an ENG metamaterial is a matrix of cells containing a thin metal wire as shown in figure 1.2. This lattice behaves as a high pass filter for an incident plane wave with an electric field parallel to the wires. The propagation is similar to the propagation in a plasma medium. The ENG metamaterial presents a plasma frequency that depends on the wires radius and the distance between two adjacent conductors (lattice constant).

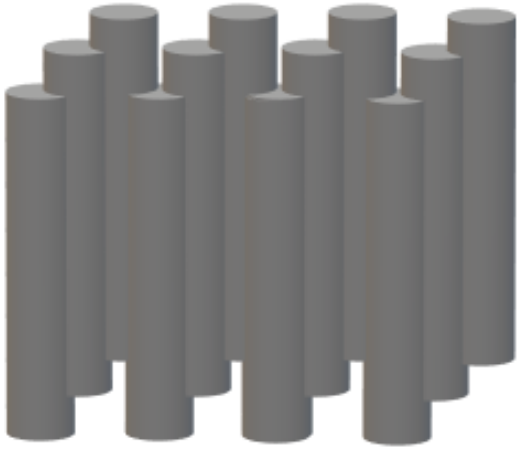

Figure 1.2: Lattice of thin metal wires working as a ENG metamaterial

This behavior can be achieved only if the lattice constant is much smaller than the wavelength.

1.3 MNG metamaterials

The most popular cell that behaves as MNG material is the split ring resonator (SRR). The cell is composed by two concentric (circular or square) rings separated by a gap. Each ring has a narrow slot that faces opposite directions (180°) as shown in figure 1.3.

Figure 1.3: Lattice of split ring resonators working as a MNG metamaterial

The rings work as an inductor and the gap behave like a capacitor. This cell behaves as an LC resonant circuit for a normal incident plane wave. The effective permeability of MNG lossless material realized by spiral ring resonators is given by equation:

$$\mu_{eff} = 1 - \frac{\omega_{mp}^2 - \omega_0^2}{\omega^2 - \omega_0^2} \tag{1.2}$$

where ω_0 is the resonation frequency and ω_{mp} is the magnetic equivalent plasma frequency. The permeability is negative for waves propagating between ω_0 and $_{mp}$ and positive above. This behavior can be achieved only if the spiral ring resonator dimension is much smaller than the wavelength.

1.4 DNG metamaterials

A DNG material could be obtained combining the ENG and the MNG cells proposed in section 1.2 and 1.3. This material presents a negative refractive index value.

$$n = \sqrt{\varepsilon_r}\sqrt{\mu_r} = -\sqrt{|\varepsilon_r|}\sqrt{|\mu_r|} = -|n| \tag{1.3}$$

This is possible if there is at least an interval of frequencies where there is a superposition of the ENG and MNG properties. The permittivity and the permeability can be described in frequency by a lossless Drude model as follow.

$$\varepsilon_{eff} = 1 - (\omega_{pe}^2)/\omega^2 \tag{1.4}$$

$$\mu_{eff} = 1 - (\omega_{pm}^2)/\omega^2 \tag{1.5}$$

If ω is lower than ω_{pe} and ω_{pm}, then the permittivity and permeability values are negative. In DNG material particular phenomenon occurs such as the negative refraction or the backward waves propagation. Further explanations can be found at [7].

1.4.1 Backward waves

Suppose an x-polarized plane electromagnetic wave propagating in a dielectric medium along the z axis. The phasors fields are the following:

$$\overline{E} = E_0 e^{-jkz}\widehat{x} \tag{1.6}$$

$$\overline{H} = H_0 e^{-jkz}\widehat{y} \tag{1.7}$$

The wavenumbers, obtained by the plane wave dispersion relation ($k^2 = \omega^2 \varepsilon_r \mu_r$), have the following values respectively in a DPS and in a DNG material:

$$k^{DPS} = \sqrt{(\omega^2 \varepsilon_r^{DPS} \mu_r^{DPS})} = \omega|n| \tag{1.8}$$

$$k^{DNG} = -\sqrt{(\omega^2 \varepsilon_r^{DNG} \mu_r^{DNG})} = -\omega|n| \tag{1.9}$$

The plane wave impedance is the same in both DPS and DNG material and it is given by equation 1.10:

$$\eta^{DPS} = \eta^{DNG} = \eta = \frac{E_0}{H_0} = \frac{k}{\omega \varepsilon_0 \varepsilon_r} = \sqrt{\frac{\varepsilon_0 \varepsilon_r}{\mu_0 \mu_r}} = \eta_0 \sqrt{\frac{\varepsilon_r}{\mu_r}} \tag{1.10}$$

The Poynting vector calculated in both media is obtained by the relation below:

$$\overline{P} = \frac{1}{2}\Re[E \times H^\star] = \frac{E_0^2}{2\Re[\eta^\star]} e^{-2\Im[k]z}\widehat{z} \tag{1.11}$$

The propagation constants have opposite sign in the two media. In the DNG material the wave phase shifts backward as if the source was in the opposite direction of the incident wave. The Poynting vector maintains the same direction in both media because of the causality principle. This phenomenon is called backward wave propagation. An exhaustive exposition can be found at [8]

1.5 ELC Resonators

Figure 1.4: three variants of Electrically coupled LC resonators

Initial DNG structures, were based on SRRs and thin-wire media [9]. However, thinwire-media metamaterials have some serious drawbacks. They require continuous electrical connections between unit cells. When the long wire is cut at the terminal of the unit cell to make each cell resonant individually, the resonance frequency is shifted to a much higher frequency. The ELC resonator, introduced by Schurig [10], serves as an alternative route to customize the value of the permittivity. Many compact ELC configurations have been introduced in recent years [11]. These designs are based on the concept of raising the overall inductance and capacitance by changing the size of the inclusion, shortening gaps, lengthening wires, or redesigning the resonator pattern to accommodate a higher capacitance or inductance. Figure 1.4 shows three different geometries of ELC resonators. As for the resonator used for this study in IHP GmbH, a structure with interdigital capacitors has been chosen, as shown in Figure 1.5. As an ELC resonator, it is expected that the value of ϵ is negative and the value of μ is positive for the bandwidth chosen. To test this behaviour an electromagnetic simulation has been run on a single cell, the curves are visible in Figure 1.6 and 1.7.

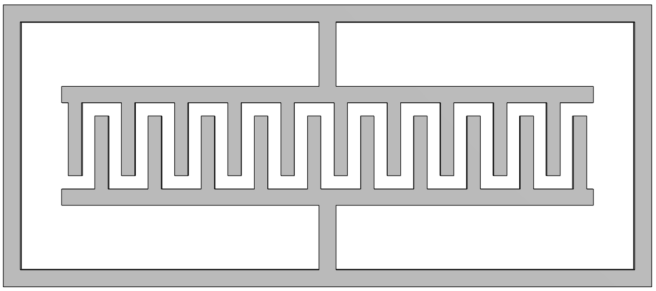

Figure 1.5: Geometry of the interdigital ELC resonator chosen

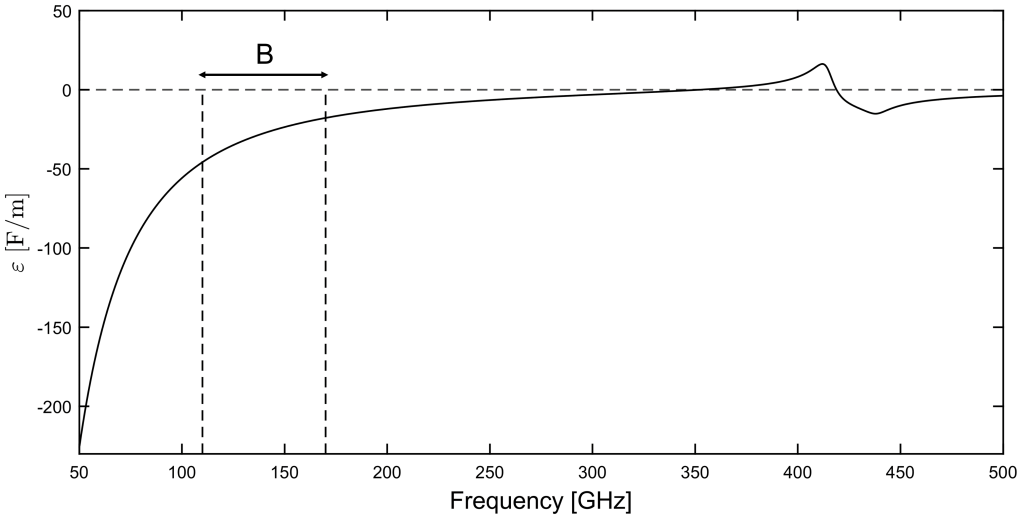

Figure 1.6: Permittivity curve

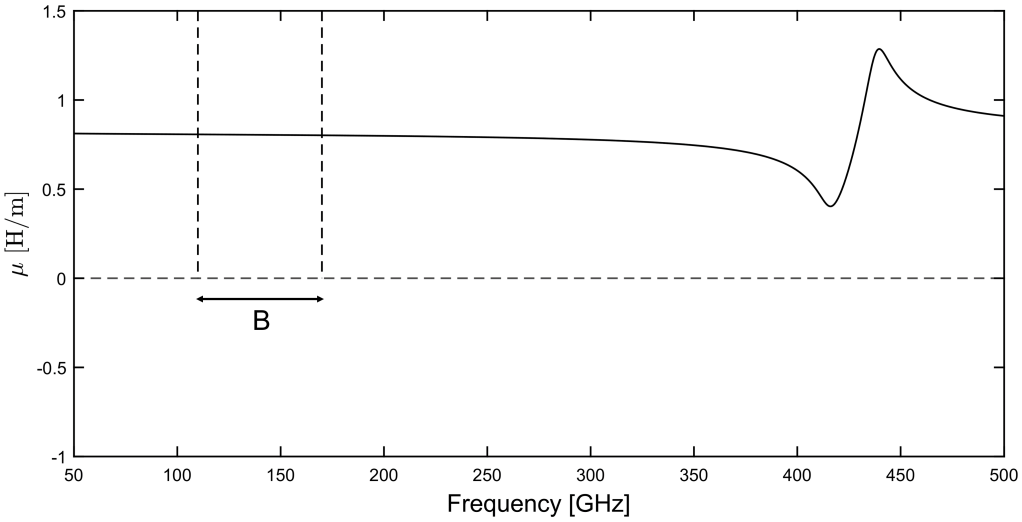

Figure 1.7: Permeability curve

As expected, in the bandwidth of interest B, ϵ is negative and μ positive. It is possible to find many studies in literature about obtaining a metamaterial with wave vector $\vec{k}$ antiparallel to the Poynting vector $\vec{P}$ with single-negative resonators [12, 13]. It is possible to say that the metamaterial that we are studying is Left-Handed.

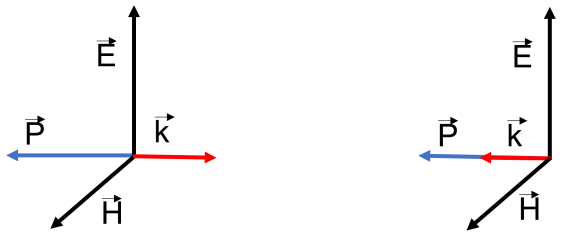

Figure 1.8: Right-Handed and Left-Handed metamaterials

Chapter 2

Production process and Measurement protocol

Contents

2.1 Production Process

In this chapter it is explained IHP's state-of-the-art 0.13- m S_iG_e BiCMOS (SG13) technology used for the production of the metamaterial transmission lines on which the simulation models are based.

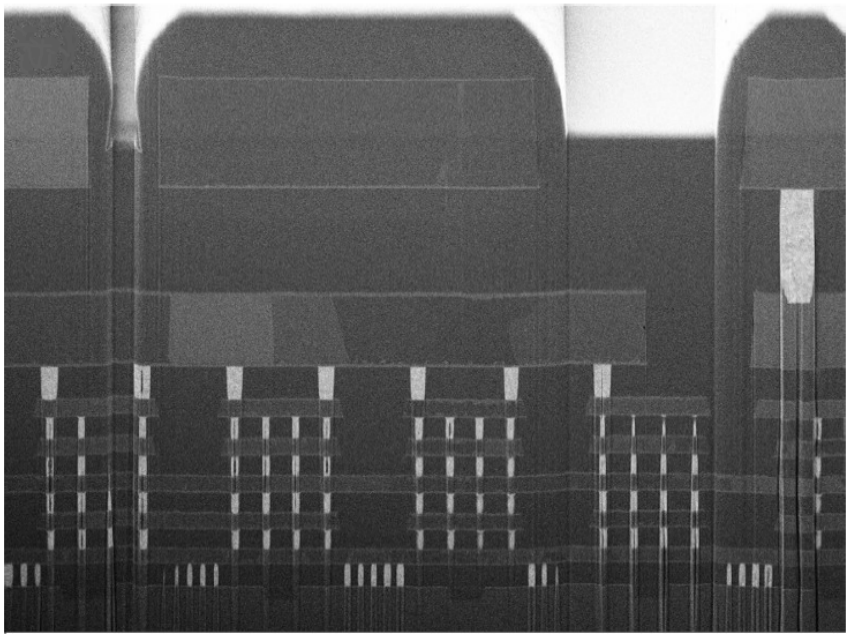

Figure 2.1: Cross section of IHP's fully processed BiCMOS wafer.

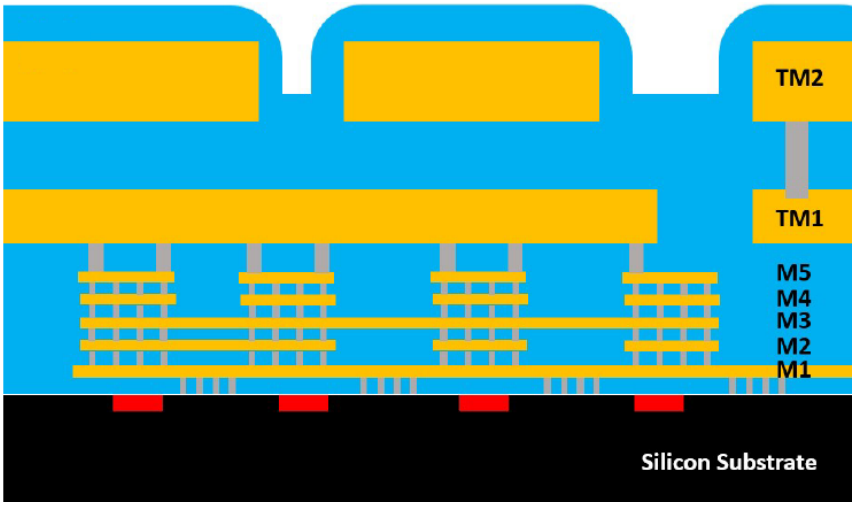

Figure 2.2: Cross section sketch

As it is shown in figure 2.1 and more clearly in figure 2.2 , the 15 μm SG13 BEOL has 7 redistribution layers in total: 5 thin metal layers (M1 to M5) and 2 thick top metal layers (TM1 and TM2). Additionally, the corresponding 6 silicon dioxide layers serve as interlayer dielectrics, and a silicon nitride passivates the top metal. After finalizing the FEOL, the tetraethyl orthosilicate (TEOS)

oxide layer is used for the passivation of the FEOL. Then, the contact vias are etched, filled with tungsten, followed by chemical mechanical polishing (CMP). After this, M1 is sputtered as the first metal layer. The 500 nm thick M1 stack consist of AlCu (99.5% Al) sandwiched between two thin Ti/TiN layers. After structuring of the M1, the ILD oxide layer is deposited and the vias are formed. Similar to the contact formation, the vias are filled with tungsten and CMP is applied. The process details of M1 RDL are depicted in Fig 3.3. Other metallization layers up to the M7 are formed the same way as M1. In between M5 and TM1, the metal-insulator-metal (MIM) capacitor is realized. Finally, the TM2 is patterned and passivated by a silicon nitride layer. Pad opening on the passivation layer to access the pads on TM2 is the last step to finalize the full BiCMOS flow [14].The entire BiCMOS flow (SG13S technology) for FEOL and BEOL has approximately 600 process steps, including the measurement steps.

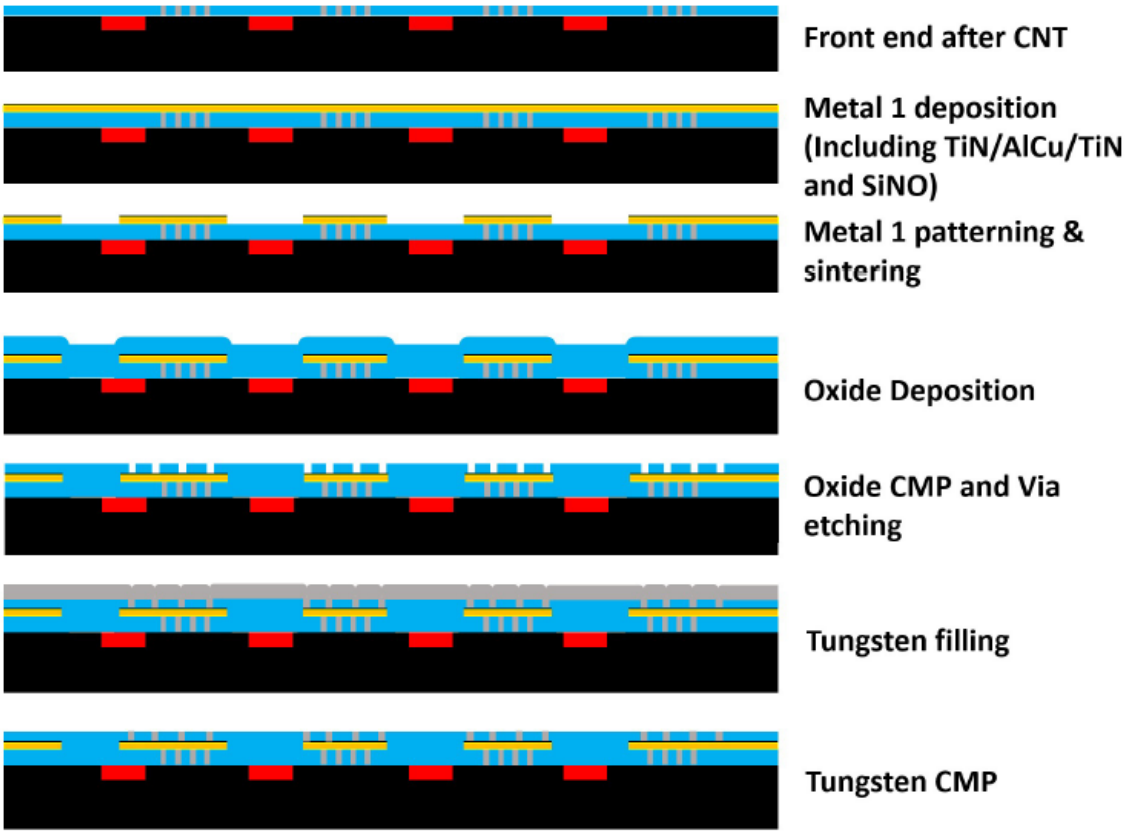

Figure 2.3: Production process

Once the production process is finished, the result is a complete transmission line with Metamaterials on the TM1 level and the actual line on the TM2 level. Various pictures were taken with both laser and optical microscope, of course only the first 2-3 layers are visible, as shown in Fig.2.4 and Fig.2.5

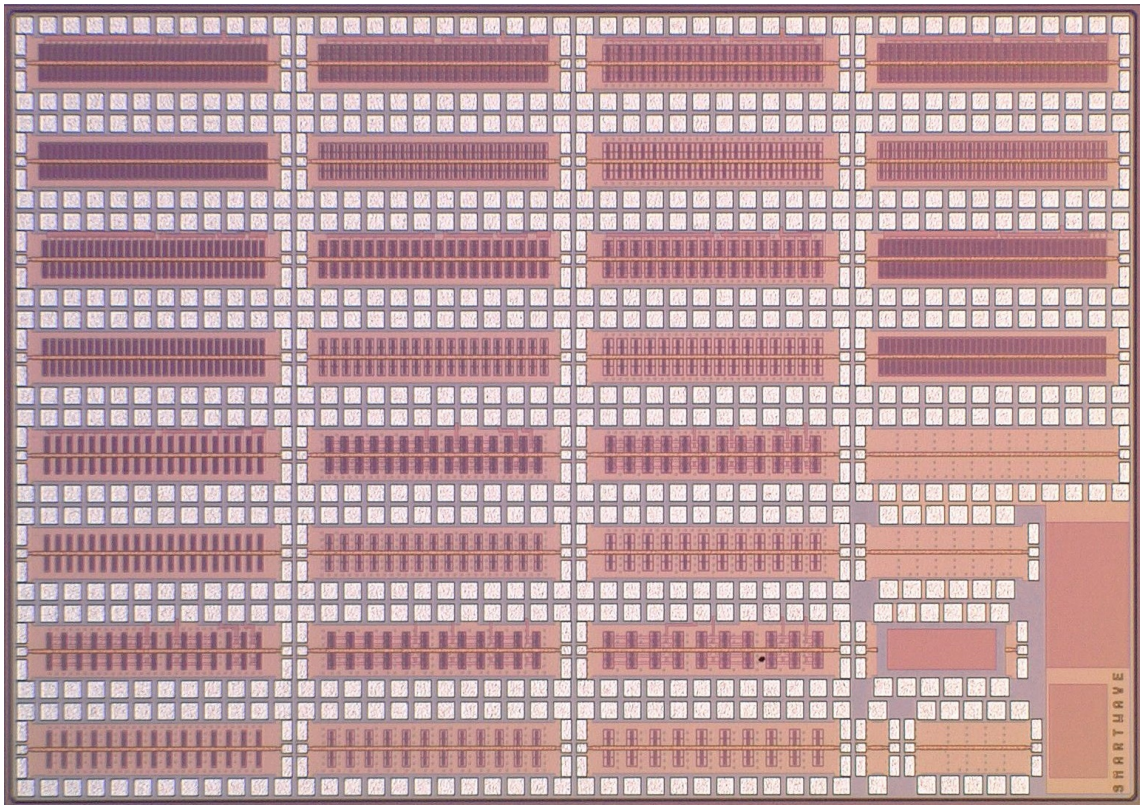

Figure 2.4: Laser microscope image of all the Transmission lines

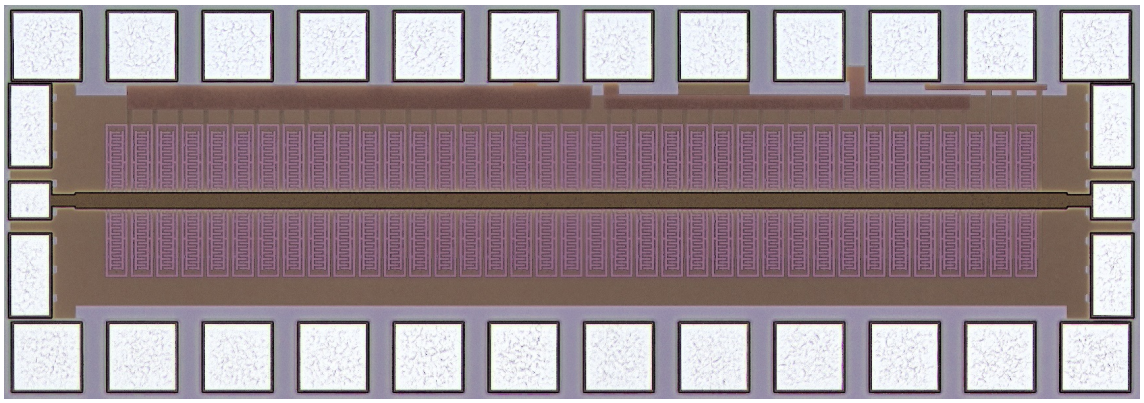

Figure 2.5: Single Transmission line (1mm total length)

2.2 Measurement Protocol

The S parameters of every transmission line are measured through a probe station. As shown in Fig.2.5, the transmission lines have a GSG(ground-signal-ground) pad configuration, this is needed since it is impossible to open a contact on both the signal line and the ground. In this pad configuration the ground pads are connected to the bottom plate thru vias, making the measurement possible.

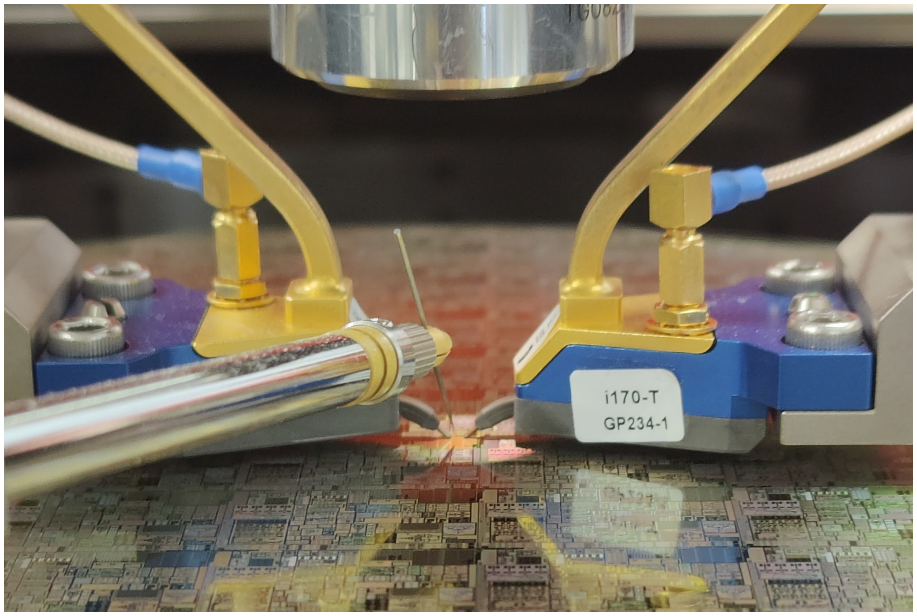

Figure 2.6: Measurement setup

Since the pads have a structure similar to a coplanar waveguide, there will be a transition segment from the pads to the line itself, this changes the behaviour of the transmission line and more specifically the reflection and transmission parameters measured. It is important to use a calibration method to de-embed the line from the pads, to ensure that only the microstrip is taken into account during the measurements.

2.3 Multi Thru Reflect Line calibration

The main problem of On-Wafer measurements is that the measured S matrix comprehends the probes used for the measurements, the pads and the transition section where the electromagnetic field commutes from a CPW configuration to a microstrip one, this has to be removed to ensure that the meaurements on the line is not compromised. An MTRL calibration is provided from the software package of MultiCal®.

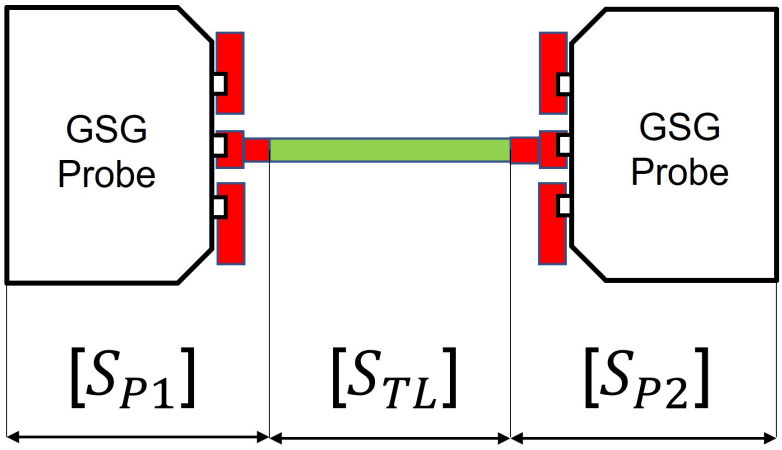

Figure 2.7: The On-Wafer calibration problem

The main goal of the Calibration is to correct the measurement by removing the $[S_{P1}]$ (S matrix of the Probe 1) and $[S_{P2}]$[15], this is done by utilizing an ensemble of uncorrected two-port S-parameter measurements collected from a set of calibration lines of different lengths that are produced on the same space on-wafer (see bottom right of Figure 2.4). The method defines transmission-line standards that differ only in length, and an arbitrary reflection standard that is considered identical for both port connections. As a key part of this process, MTRL estimates the propagation-constant of the standards frequency-by-frequency, then computes the S parameter correction coefficients in two parts, using the accurate estimate of the propagation constant [16]. This method simplifies the modeling of the line, it is in fact possible to avoid considering the influence of the pads and the probes, focusing only on the line itself. To grant the reliability of the measures, the process is repeated on multiple areas of the same Wafer. As for the band of interest, we consider the band 110-170 GHz, which is the band that the instrument allows without changing radically the setup.

Chapter 3

Model Implementation

Contents

3.1 Phase Shifters

In physics the phase of a periodic function F of some real variable t (such as time) is an angle-like quantity, denoted by $\phi(t)$, representing the fraction of the cycle covered up to t. If we consider two sinusoidal signals $G(t)$,$F(t)$ as our periodic functions, the difference between the two phases at a given t:

$$\psi(t) = \phi_G(t) - \phi_F(t) \tag{3.1}$$

is called *phase shift* of G relative to F.

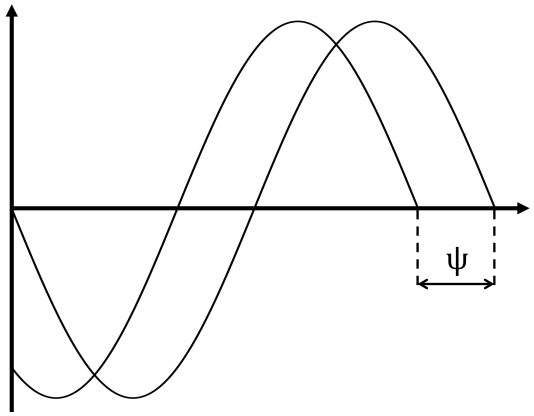

Figure 3.1: Graphic example of phase shift between two sinusoidal curves

Phase shift is a common term in the study of waveforms, it refers to the displacement of two signals in a time domain. When the signals have opposite signs, destructive interference occurs, when the phase difference $\psi(t)$ is $(n+1/2)\pi$, sinusoidal signals are said to be in phase quadrature. It is important to understand that phase shift does not change the frequency of the signal. Phase Shifters are used to change the transmission phase angle of an input signal. Ideally, a phase shifter provides an output signal with an equal amplitude to the input signal, any loss here will be accounted to the insertion loss of the component. The input signal is shifted in phase at the output based on the phase shift provided. At microwave frequencies, phase shifters can be designed using ferromagnetic materials for obtaining switchable phase shift, semiconductor, or Metamaterial based devices. In comparison with ferrite realizations, phase shifters based on semiconductor or metamaterials devices are more compact, have lower switching times and require lower drive power [17]. Recently, composite left-handed transmission lines have been used to design compact phase shifters, the name left-handed is because the direction of the Poynting vector is antiparallel to the direction of phase velocity and, thus, the vectors $\vec{E}$, $\vec{H}$ and $\vec{k}$ form a left-handed triplet [18, 19].

3.2 Metamaterial model

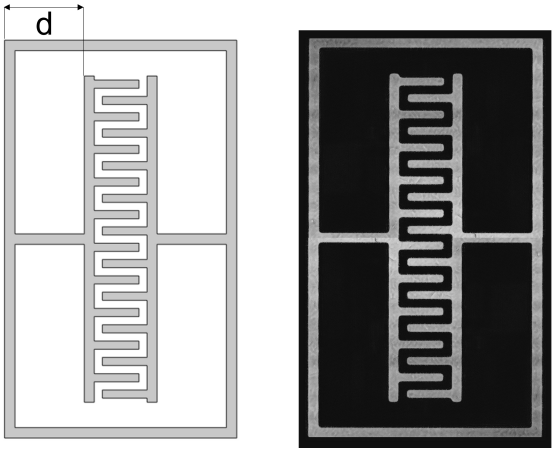

Figure 3.2: Right: COMSOL Geometry Left: laser microscope image

All the models are implemented in Comsol Multiphysics®, using the frequency domain module. The first model implements a single metamaterial cell as shown in Fig.3.2. The geometry is made so that the variation of the single parameter d modifies the structure accordingly. For this study, the values for d are $4\mu m$,$10\mu m$ and $16\mu m$. As for the material, aluminium has been used, the electrical conductivity σ is 2.78e7 $[S/m]$. An electromagnetic simulations on a single cell has been performed to show the lines of the electric field in the structure(Fig.3.3). Since the cells are disposed on a plane under a microstrip line, a fair approximation of an incident field can be done considering an excitation perpendicular to the cell.

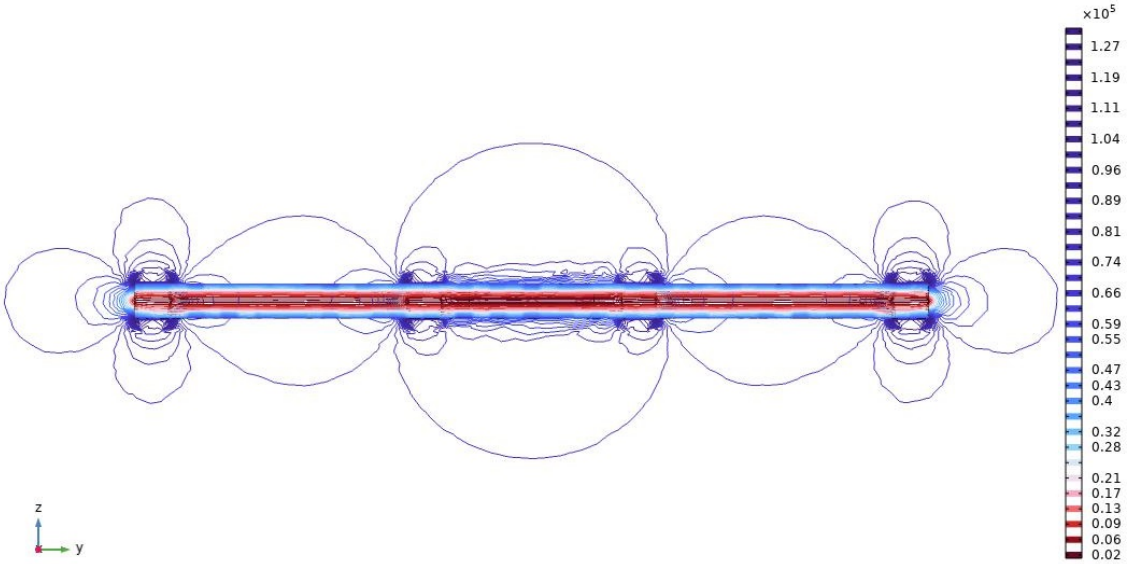

Figure 3.3: Electric field lines of a single cell with an incident field E_z at a frequency of 150Ghz

3.3 Transmission Line Model

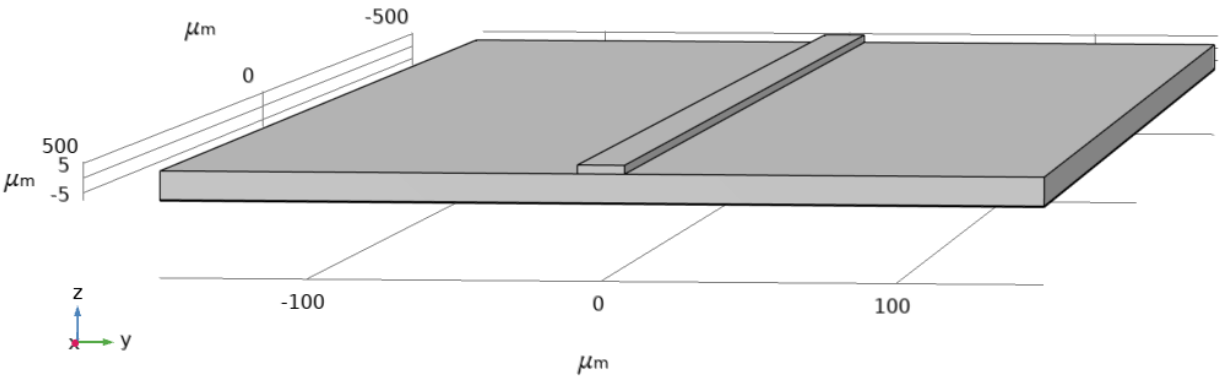

Figure 3.4: Geometry of the microstrip model

A microstrip line is used as the base transmission line for the structure, a simple model of a microstrip with base ground is shown in figure 3.4. The parameters for the geometry are shown in the table below.

Parameters	**Value**
Line length	1000 μm
Line width	16 μm
Line thickness	3 μm
Dielectric thickness	9.77 μm
Ground thickness	0.42 μm

The materials are silicon oxide (S_iO_2) for the semiconductor, with relative permittivity ϵ of 4.1, and Aluminium (Al) for the microstrip and ground, electrical conductivity σ of 3.03e7 $[S/m]$. Thanks to the MTRL calibration, it has been possible to build the geometry of the line ignoring the pads. The same geometry is going to be used for the final model of the phase shifter.

3.4 Phase Shifter Model

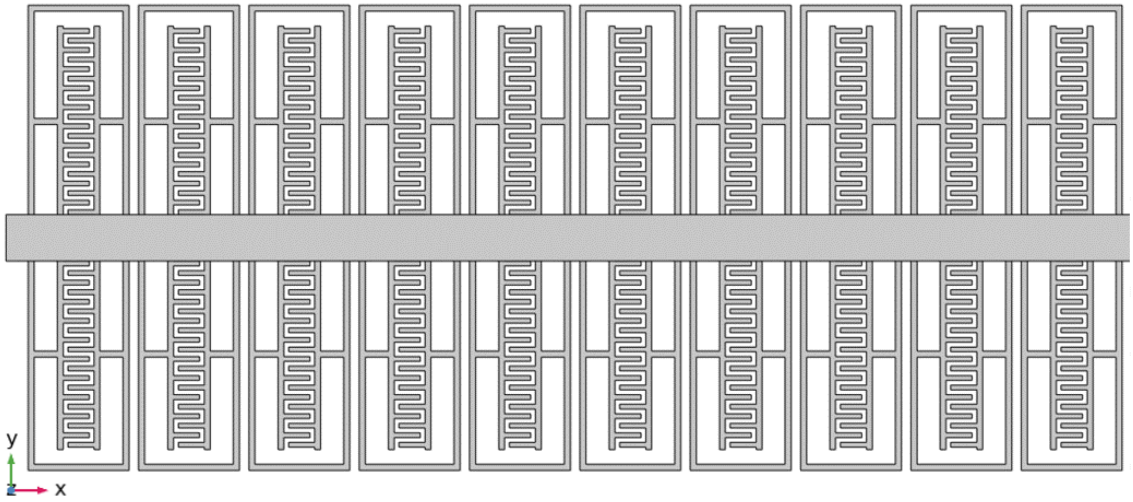

Figure 3.5: Top view of a combined model section (ground and dielectric hidden)

As the final model of the transmission line, the previous models have been combined. The resonators are disposed in symmetrical couples under the microstrip. The system made of the line and the cells is embedded in silicon dioxide and has a ground plane on the bottom. The parameters of the geometry follow the production guideline and are shown in the table below.

Figure 3.6: front view of the model

Parameter	Value
Cell thickness	2 μm
Cell-Line distance	2.8 μm
Cell-Ground distance	4.97 μm
Dielectric height	14.69 μm
Ground thickness	0.42 μm

For the simulation, the Boundary Mode Analysis study is used. This method computes the propagation constants as well as propagating mode shapes, for a given frequency at a port. As a study, the Boundary Mode Analysis combines a Boundary Mode Analysis study step at a port, which can represent a cross section of a waveguide, with a Frequency Domain study for the full geometry. The results of the simulations are discussed in chapter 4.

Chapter 4

Results

Contents

4.1 Simulation results

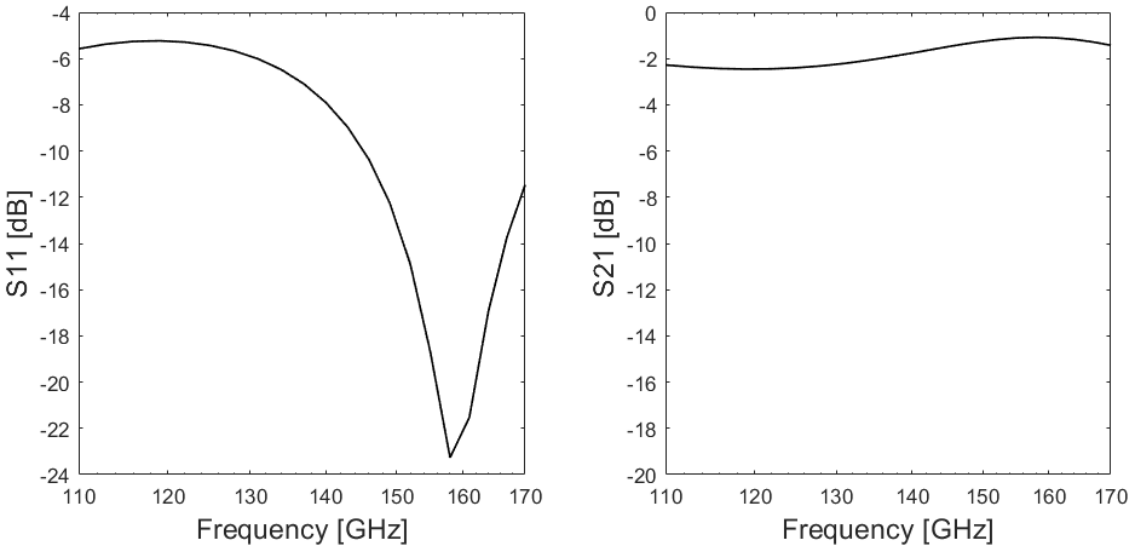

Figure 4.1: S parameters obtained from the simulation of a microstrip

Figure 4.1 shows the S parameters of a simple microstrip line embedded in S_iO_2 dielectric, the dimensions are the same as the case with the cells.The bandwidth is from 110 GHz to 170 GHz to match the range of the measurement, this allows to do a proper comparison of the results later. As expected, the reflection indice S11 is low, while the losses represented by the S21 are not absent, this is probably because the materials used in the simulations has the same properties of the one used in the production process, so it is not ideal and can develop losses at high frequencies. Figure 4.2 instead shows the S11 and S21 simulation results of a phase shifter. Looking at the S21, it is possible to see how the behaviour of the losses change inserting meta-materials in the structure.

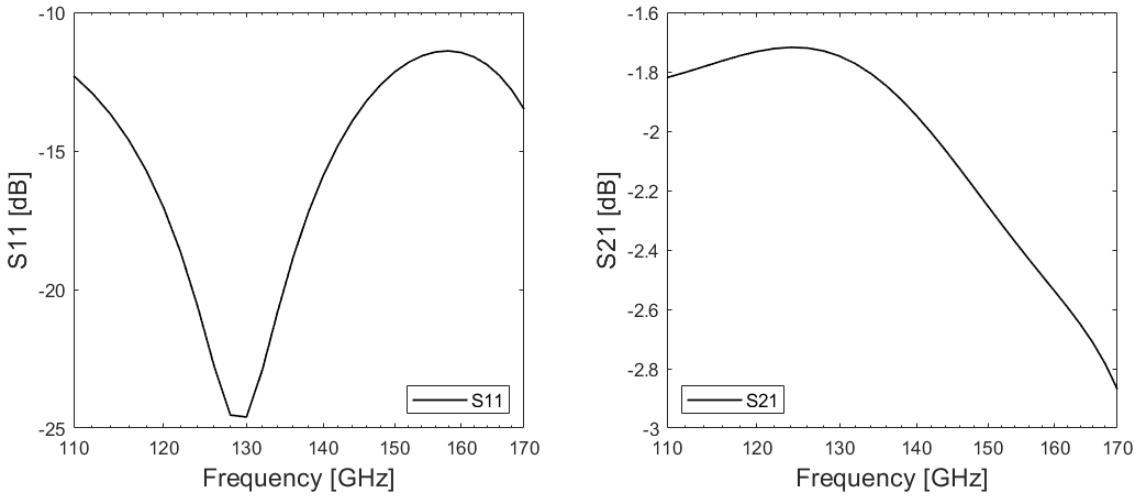

Figure 4.2: S parameters obtained from the simulation of the phase shifter

4.2 Measurement data

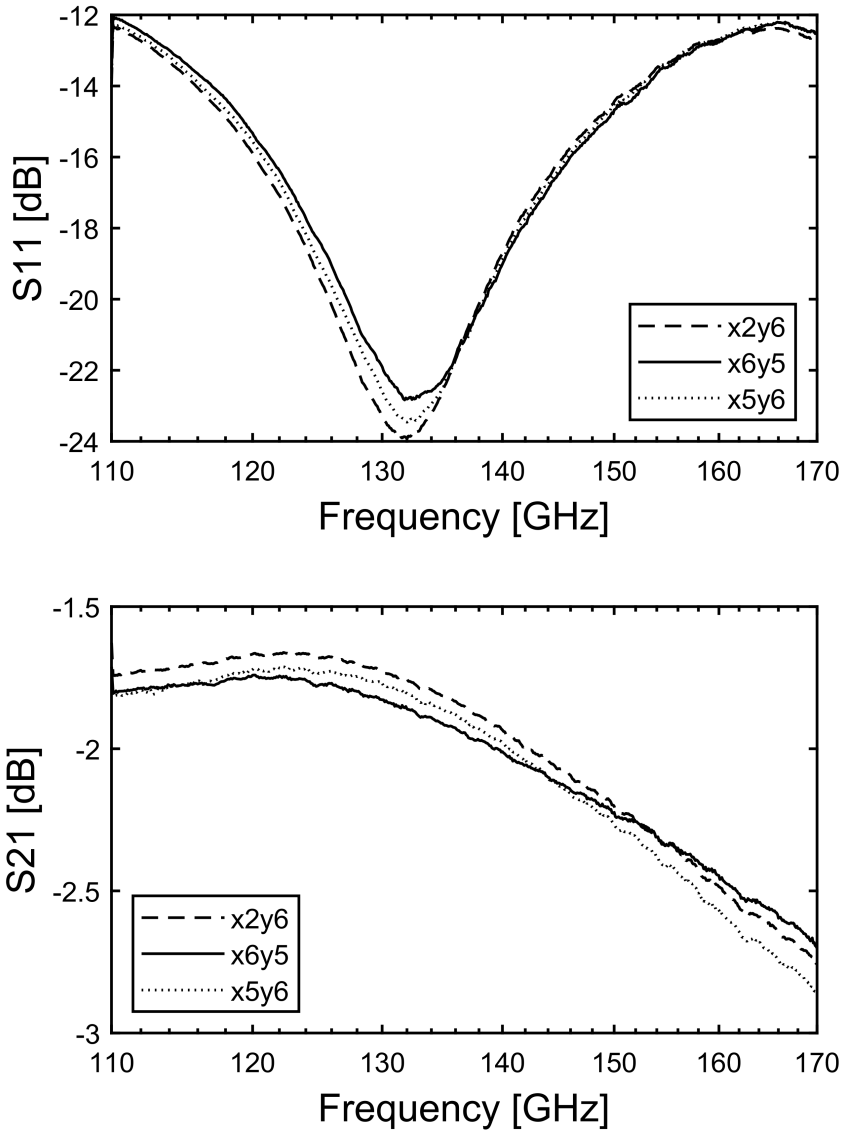

Figure 4.3: S parameters from measurement, different curves belong to different areas of the Wafer

The S parameters obtained from the measurement protocol discussed in chapter 2 are shown in Figure 4.2, since the array of structures is produced multiple times on the same wafer, multiple measurements of every transmission line have been performed. This is done because even if the production process is extremely precise, it is possible to find a defective transmission line or a production flaw in some sections of the wafer. In the figure, 3 plots of the same phase shifter are shown, it is possible to see how the curves don't sensibly change from a section to another, with sections addressed with x and y coordinates in a grid.

4.3 Simulation-measurement comparison

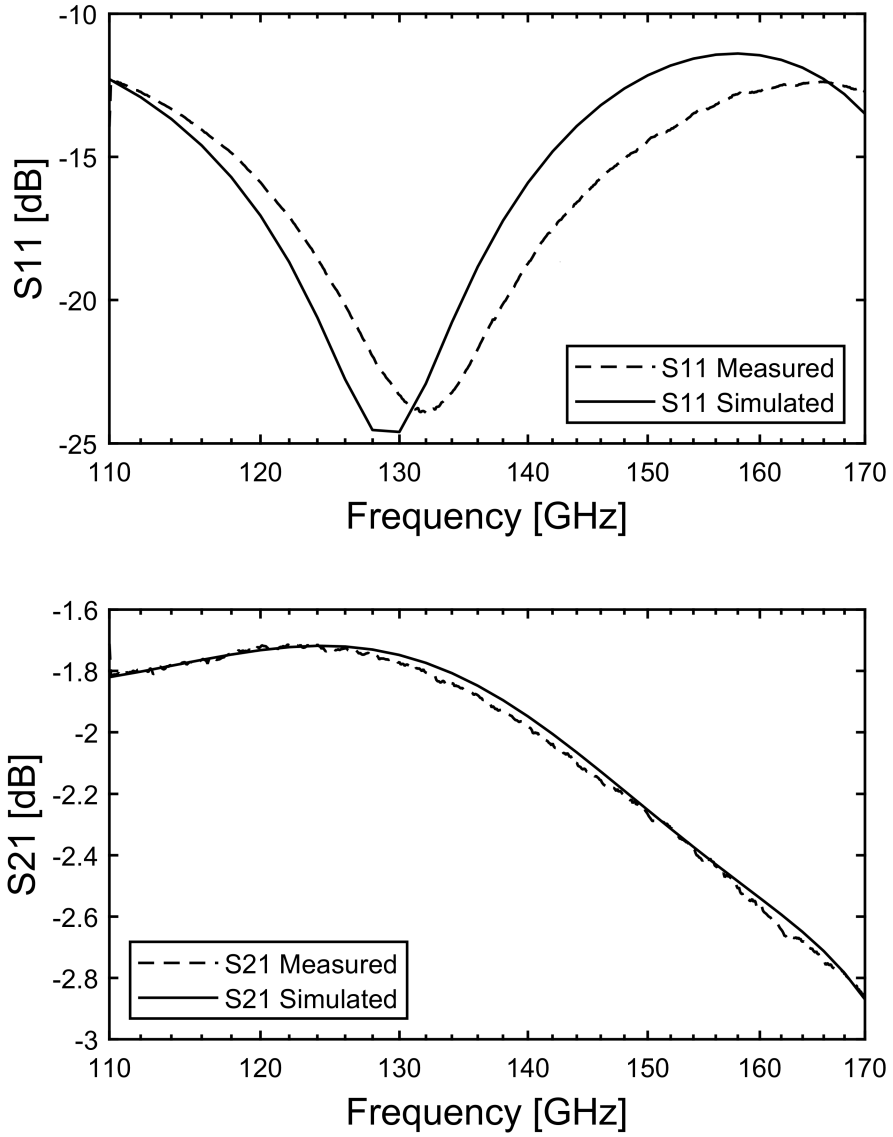

Figure 4.4: S parameters comparison

It is possible now to plot the curves to have a comparison. In chapter 4.2 is shown how the measurement are similar in different sections of the wafer, so it's possible to pick any curve regarding a given transmission line for the comparison. The transmission line picked has metacells with d=10μm, see chapter 3, similar results are obtained from structures with different d. As shown in Figure 4.4, the simulation results match the measurement data, proving that the MTRL calibration is effective and the model is coherent with the real structure.

4.4 Phase Shifting

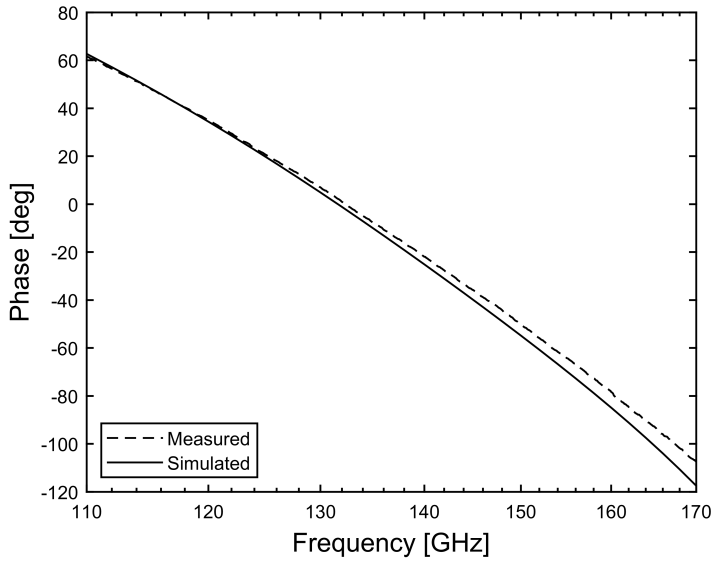

Figure 4.5: Phase of the measured line vs Phase of the simulated one

For what concerns the phase, two comparison are needed, the first is between the phase of the simulated phase shifter and the measurement of the producted one, to evaluate the quality of the simulation. The second is between the simulation of the microstrip without the meta-cells and the one with the meta-cells included in the structure, to have a view of how the phase changes with the variation of the dimensions of the metamaterials and with the numerosity of them under the microstrip. Figure 4.5 shows the curve of a simulated phase shifter and the one obtained from the measurement data, it is clear that the simulations fit almost perfectly the real behaviour of the producted line. Rising the frequency a small difference appear between the two curves, the maximum difference is though around 7°, this could be caused by the non ideality of the real material, but it is small enough to be considered negligible. At this point it is possible to analyze the behaviour of the phase shifters respect to the microstrip line considering only the curves obtained from the simulations, Figure 4.6 shows a comparison of the curves of structures with different d lengths and similar number of metacells.

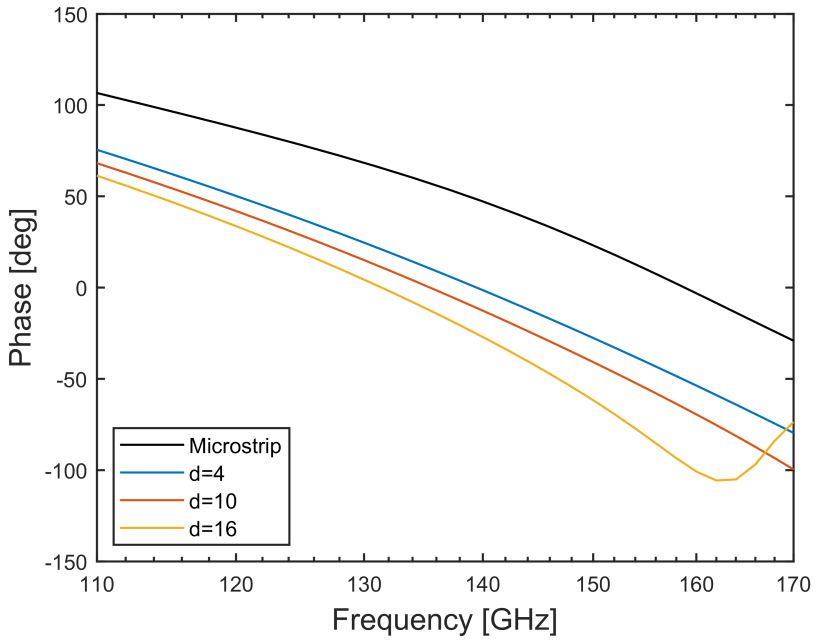

Figure 4.6: Curves of the phase for structures with different cell dimensions

The curves in Figure 4.6 represent the phase variation of the structures with different cell dimensions given a fixed number of cells under the line, in this case, only the structures with 15 couples of metacells are taken in consideration. It is possible to see how the phase of a given frequency changes drastically with the presence of metacells, at 140 GHz the difference in phase arrives at 90° respect to the normal microstrip. For the metacells with d=16μm the curve has a maximum at around 160 GHz, this can be caused by superior modes that can be excited at that frequency even if the initial excitation is a quasi-TEM mode. Alternatively, it is possible to fix a certain dimension d and increase the number of cells, figure 4.7 shows the behaviour of phase shifters with d=10μm and variable number of cells.

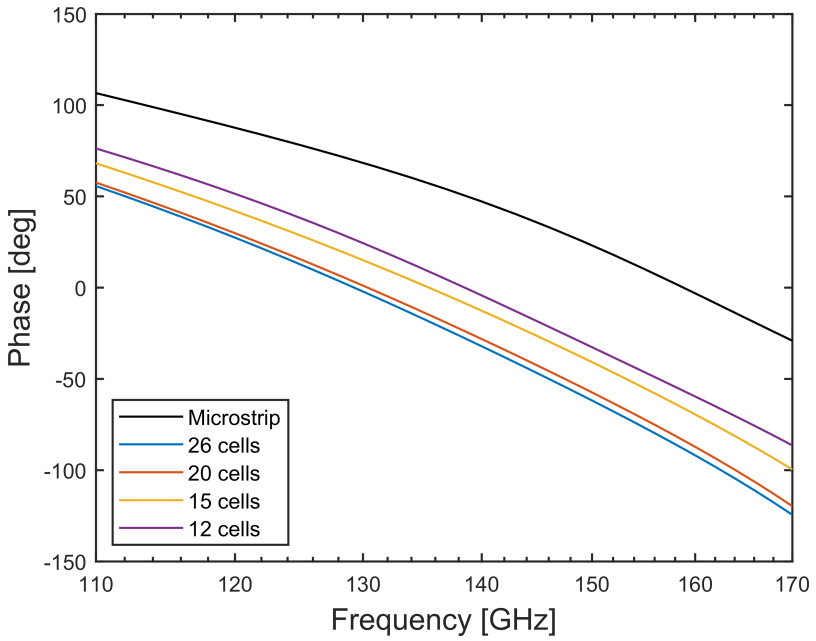

Figure 4.7: Curves of the phase for structures with different cell numerosity

The shift of the phase goes higher incresing the number of cells, but it is clear that the difference between the structure with 20 and 26 cells is particularly small. This is probably due to the interaction between the cell with the near ones, since the length of the line is fixed, increasing the number of cells simply means that the distance between cells decreases accordingly. If the cells get too near, it is plausible that every cell absorbs a part of the fields radiated from the near ones, reducing the effect on the microstrip.

Conclusion

This thesis had the objective to present the production process, the measurement protocol but most importantly the multiphysics model of a phase shifter based on metamaterials. According to the results in chapter 4, the results of the theoretical-numerical model match the experimental results of the real device with high accuracy. In particular, it is possible to evaluate and predict the phase-shifting behaviour in terms of dimensions and number of metacells. Taking into account the reduction of the wavelength, it is possible to use a physical line that is 30% shorter respect to a line without metamaterials, granting better performance, i.e.lower power consumption, reduced capacitive coupling and cross-talk. This work is a preliminary but fundamental study for the design of ELC-metamaterial based phase-shifters; the next step consists in the introduction the tunability of the cells to modify the phase characteristics.

References

[1] Irina B. Vendik and Orest G. Vendik. "Metamaterials and their application in microwaves: A review". In: *Technical Physics* 58 (2013), pp. 1–24.

[2] Christophe Caloz and Tatsuo Itoh. "Metamaterials for High-Frequency Electronics". In: *Proceedings of the IEEE* 93 (Nov. 2005), pp. 1744–1752. DOI: 10.1109/JPROC.2005.853540.

[3] R. Marques, Ferran Martín, and Mario Sorolla. *Metamaterials with Negative Parameters: Theory, Design and Microwave Applications*. Jan. 2008. DOI: 10.1002/9780470191736.

[4] Benjamin D. Braaten et al. "A cascaded reconfigurable RH/CRLH-zero-phase microstrip transmission line unit cell". In: (2012). DOI: 10.1109/ICWITS.2012.6417783.

[5] F. Ellinger, H. Jackel, and W. Bachtold. "Varactor-loaded transmission-line phase shifter at C-band using lumped elements". In: *IEEE Transactions on Microwave Theory and Techniques* (2003). DOI: 10.1109/TMTT.2003.809670.

[6] C. Weil et al. "Ferroelectric- and liquid crystal- tunable microwave phase shifters". In: *33rd European Microwave Conference Proceedings (IEEE Cat. No.03EX723C)*. 2003. DOI: 10.1109/EUMC.2003.177757.

[7] Richard W. Ziolkowski Nader Engheta. "Metamaterials: Physics and Engineering Explorations". In: Wiley-IEEE Press, 2006. Chap. 1. ISBN: 978-0-471-76102-0.

[8] R.W. Ziolkowski and Ehud Heyman. "Wave Propagation in Media Having Negative Permittivity and Permeability". In: *Physical review. E, Statistical, nonlinear, and soft matter physics* 64 (Dec. 2001), p. 056625. DOI: 10.1103/PhysRevE.64.056625.

[9] Pendry et al. "Extremely low frequency plasmons in metallic mesostructures." In: *Physical review letters* (1996).

[10] D. Schurig, J. J. Mock, and D. R. Smith. "Electric-field-coupled resonators for negative permittivity metamaterials". In: *Applied Physics Letters* (2006). DOI: 10.1063/1.2166681.

[11] Withawat Withayachumnankul, Christophe Fumeaux, and Derek Abbott. "Compact electric-LC resonators for metamaterials". In: *Opt. Express* (2010). DOI: 10.1364/OE.18.025912. URL: http://opg.optica.org/oe/abstract.cfm?URI=oe-18-25-25912.

[12] Ferran Martín. *Artificial Transmission Lines for RF and Microwave Applications*. July 2015, pp. 1–526. ISBN: 9781118487600. DOI: 10.1002/9781119058403.

[13] F. Aznar et al. “Characterization of miniaturized metamaterial resonators coupled to planar transmission lines”. In: *Journal of Applied Physics* 104 (Jan. 2009), pp. 114501–114501. DOI: 10.1063/1.3021109.

[14] Zhibo Cao et al. “An Advanced Finite Element Model for BiCMOS Process Oriented Ultra-Thin Wafer Deformation”. In: *IEEE Transactions on Semiconductor Manufacturing* (2022). DOI: 10.1109/TSM.2021.3132550.

[15] Donald Degroot, J.A. Jargon, and R.B. Marks. “Multiline TRL revealed”. In: Jan. 2003, pp. 131–155. ISBN: 0-7803-8124-6. DOI: 10.1109/ARFTGF.2002.1218696.

[16] D.F. Williams, C.M. Wang, and Uwe Arz. “An optimal multiline TRL calibration algorithm”. In: *IEEE MTT-S International Microwave Symposium Digest, 2003* 3 (2003), 1819–1822 vol.3.

[17] “10 - Fiber, holographic, quantum optical and other types of optical switches”. In: *Optical Switches*. Ed. by Baojun Li and Soo Jin Chua. Woodhead Publishing Series in Electronic and Optical Materials. Woodhead Publishing, 2010. ISBN: 978-1-84569-579-8. DOI: https://doi.org/10.1533/9780857090416.276.

[18] M.A. Antoniades and G.V. Eleftheriades. “Compact linear lead/lag metamaterial phase shifters for broadband applications”. In: *IEEE Antennas and Wireless Propagation Letters* (2003). DOI: 10.1109/LAWP.2003.815280.

[19] Michael Maassel, Benjamin D. Braaten, and David A. Rogers. “A metamaterial-based multi-band phase shifter”. In: *IEEE International Conference on Electro/Information Technology*. 2014. DOI: 10.1109/EIT.2014.6871820.